Electronic Supplementary Material (ESI) for Journal of Materials Chemistry C.


# Cu/Ni Keggin-Based Viologen Complexes with Water-Assisted 1D Proton Channel for Asymmetric Supercapacitors

Hongtao Cui[a], Tao Liu[b], Mengle Yang*[a], Aixiang Tian[a], Jun Ying[a], Xiuli Wang[a]*

a College of Chemistry and Materials Engineering, Bohai University, Jinzhou, 121013, P. R. China.

b College of Sciences, North China University of Science and Technology, Tangshan, Hebei 063210, China.

*Corresponding authors: yangmengle@bhu.edu.cn; wangxiuli@bhu.edu.cn

## Experimental section

### Materials

### Materials and general methods

All reagents are used without further purification. All syntheses of the coordination polymers are carried out in 25 mL polytetrafluoroethylene lined stainless steel containers under autogenous pressure. Mill-Q water (18.2 MΩ cm resistance) is used to prepare all solutions in this work. The X-ray photoelectron spectroscopy (XPS) measurements were performed by a Thermo ESCALAB 250Xi spectrometer with monochromated Al Kα radiation (hγ = 1486.6 eV). All XPS spectra were calibrated with respect to the C 1s peak at 284.8 eV. The $N_2$ adsorption-desorption isotherm was conducted by using a Micromeritics Tristar II. The samples were outgassed for 10 h at 150 °C under vacuum before the measurements. The morphology and microstructure of the samples were characterized by field emission scanning electron microscopy (FE-SEM) (Hitachi, SU8000). Energy dispersive spectroscopy (EDS) data was collected with an ensemble measurement in the FE-SEM. The FT-IR spectra are recorded from KBr pellets in the range of 4000-400 $cm^{-1}$ with a Bruker OPTIK GmbH-Tensor II spectrometer (KBr disk). The powder X-ray diffraction (PXRD) patterns are obtained with a Rigaku D/max 2500 V PC diffractometer with Cu-Kα radiation, and the scanning rate is 5° $s^{-1}$, 2θ ranging from 5 to 50°. The electrochemical measurements were performed with a CHI 660 electrochemical workstation. A conventional three-electrode system is used with a saturated calomel electrode (SCE) as reference electrode and a Pt wire as counter electrode. Glassy carbon electrode (GCE) is used as the working electrodes.

### X-ray Crystallographic Study

X-ray diffraction analysis data for complexes **1** – **5** are collected with a Bruker Smart Apex CCD diffractometer with MoKα (λ = 0.71073 Å) at 293 K. All crystal structures are solved by direct methods and refined on $F^2$ by full matrix least-squares methods using the OLEX II package. A summary of the crystallographic data and structural determination for four complexes are given in Table S1. Selecting bond

lengths and angles are listed in Table S2. CCDC numbers：2328435 (**1**), 2328437 (**2**), 2112441 (**3**), 2328517 (**4**), 2328519 (**5**). These data can be obtained free of charge from The Cambridge Crystallographic Data Centre via www.ccdc.cam.ac.uk/data_request/cif.

**Ultraviolet photoelectron spectroscopy (UPS) measurements**

Ultraviolet photoelectron spectroscopy (UPS) measurements were performed with an He hυ (21.22 eV) line as an excitation source. The work function was examined by the secondary electron cut-off ($E_{cutoff}$) in the UPS spectrum. The work function (Φ) is calculated with the **eq. S1**.

$$\Phi = h\upsilon - E_{cutoff} \quad \textbf{(eq. S1)}$$

**Proton conductivity measurements**

Pellets of 13 mm in diameter and 0.85–0.95 mm thickness were prepared by pressing the complexes (about 30 mg) at 40 kN $cm^{-2}$. The proton conductivities of all the samples were estimated in quasi-four-probe method conductivity cells by the AC impedance spectroscopy technique. The S3 impedances were measured with a frequency response analyzer/potentiostat (Princeton Applied Research PAR 2273, EG&GPARC, Princeton, NJ) over a frequency range from 0.1 Hz to 1 MHz, 10 mV ac perturbation and 0.0 V dc rest voltage. The samples were covered with silver paint to improve contact with the two copper blocking electrodes in a measurement cell and placed in a temperature and humidity controlled environment. The samples were placed in closed chambers with ~97 % relative humidity (RH) levels generated by the $K_2SO_4$ standard saturated aqueous salt solution.[1] This humidity chamber is made of glass and has dimensions 19 cm height and 6 cm diameter. The saturated $K_2SO_4$ solutions were placed in the chambers for 3 days to ensure that the air in the bottle reached equilibrium. The temperature was recorded in close proximity to the membrane with a K-type thermocouple in order to measure the temperature dependence of the conductivity. The impedance studies were performed in the temperature range 298-323 K. The Nyquist plot obtained from impedance measurement comprises a depressed semicircular arc at high frequency and a spur at low frequency. The high frequency arc can be attributed to the bulk electrolyte resistance and the low frequency spur is possibly related to

electrode-electrolyte interfacial impedance.[2] The conductivity (σ, S $cm^{-1}$) of the sample was calculated from the impedance data, using the relation:

$$\sigma = \frac{l}{AR} \qquad \textbf{(eq. S2)}$$

where l (cm) is the thickness of the sample, A ($cm^2$) is the face area and R (Ω) is the sample resistance estimated as the crossing point with the real axis extrapolated from the high-frequency arc.[3] The measurements were repeated three times to get reproducible results.

**Hole mobility measurements**

The hole mobility of the complex **1**, **3** and **4** are measured using the Bruce-Evans-Vincent test method, we assembled symmetric supercapacitor devices (**1//1** SSC, **3//3** SSC, and **4//4** SSC) to explore the electron transfer properties of complexes **1**, **3**, and **4**. The bulk resistance before and after polarization of the battery were measured by an AC impedance method. Five minutes after the initial impedance measurement, a polarization test was performed by applying a voltage of 25 mV for 3600 s, and the current changes over time were recorded. Finally, the impedance of the polarized battery was tested. The electron mobility is calculated with the **eq. S3**:

$$t = \frac{I_s(\Delta V - I_0 R_0)}{I_0(\Delta V - I_s R_s)} \qquad \textbf{(eq. S3)}$$

where $I_0$ is the initial current, $I_s$ is the steady-state current, $R_0$ is the interfacial resistance before polarization, $R_s$ is the interfacial resistance after polarization.

The impedance values obtained for the three SSCs were measured before and after polarization, with an applied potential difference of 25 mV/s.

**Electrochemical Measurements**

Cyclic voltammetry (CV), galvanostatic charge−discharge (GCD) measurements, and electrochemical impedance spectroscopy (EIS) are carried out on a CHI 660 electrochemical workstation in 0.5 M $H_2SO_4$ solution under traditional three-electrode system. The working electrodes are fabricated by the mixture of the title complexes and acetylene black in a certain ratio with isopropanol and water. Then, the mixture (5 μL)

is dripped onto the surface of glassy carbon electrode (GCE). The as-prepared GCE is the working electrode, the saturated calomel electrode is used as a reference electrode, and a Pt wire acts as the counter electrode. Electrochemical impedance spectroscopy (EIS) measurements are conducted from $10^6$ Hz to 0.01 Hz with the amplitude of 5 mV referring to the open-circuit potential. GCD tests are carried out at different current densities in the range 1 to 20 A $g^{-1}$. The specific gravimetric capacitance value can be calculated from the equation:

$$Cs = \frac{I\Delta t}{m\Delta V} \quad \textbf{(eq. S4)}$$

$$Ca = \frac{I\Delta t}{S\Delta V} \quad \textbf{(eq. S5)}$$

where Ca (mF $cm^{-1}$), Cs (F $g^{-1}$), I (A), $\Delta V$ (V), $\Delta t$ (s) and m(g) represent the specific capacitance, the discharge current, potential change, the discharge time and the amount of active material on the electrode, respectively. The cycling stabilities are evaluated by carrying out multiple charge/discharge cycles.

The energy E (Wh $kg^{-1}$) and power P (W $kg^{-1}$) densities of the ASC device can be obtained from the following equations:

$$E = \frac{Cs\Delta V^2}{2 \times 3.6} \quad \textbf{(eq. S6)}$$

$$P = \frac{3600 \times E}{\Delta t} \quad \textbf{(eq. S7)}$$

Energy efficiency from galvanostatic charge-discharge curve

$$\text{Energy efficiency (\%)} = \frac{E(discharge)}{E\ (charge)} \quad \textbf{(eq. S8)}$$

$SiMo_{12}O_{40}^{4-} + nH^+ + ne^- \leftrightarrow H_nSiMo_{12}O_{40}^{4-}$ **(eq. S9)**

$GeMo_{12}O_{40}^{4-} + nH^+ + ne^- \leftrightarrow H_nGeMo_{12}O_{40}^{4-}$ **(eq. S10)**

where n is equal to 2, 4, 6.

**Material Synthesis**

**Synthesis of $[Cu_2(L_1)_4(L_2)(H_2O)_4(SiMo_{12}O_{40})_2]\cdot 8H_2O$ (1)**

A mixture of $(NH_4)_6Mo_7O_{24}\cdot 4H_2O$ (0.1 g, 0.08 mmol), $CuCl_2\cdot 2H_2O$ (0.1 g, 0.59 mmol), $L_1$ (0.02 g, 0.07 mmol), $L_2$ (0.01 g, 0.06 mmol), $Na_2SiO_3$ (0.06g, 0.49mmol) and $H_2O$ (15 mL) is stirred for 2 h in air at room temperature. The pH is adjusted to about 3.6 with 1.0 M $HNO_3$, and then the suspension is transferred to a Teflon lined autoclave and keep at 120 $^oC$ for 7 days. The temperature is reduced to room temperature with a rate of 10 $^oC$ per hour. The dark green block crystals of **1** are obtained (yield 44% based on Mo). Anal. calcd. for $C_{82}H_{92}Cu_2Si_2Mo_{24}N_{10}O_{96}$ (5239.50): C 18.87, H 1.70, N 2.68 %. Found: C 18.88 H 1.69, N 2.70 %.

**Synthesis of $[Cu_2(L_1)_4(L_2)(H_2O)_4(GeMo_{12}O_{40})_2]\cdot 8H_2O$ (2)**

The synthetic process of complex **2** is similar to complex **1** except for the replacement of $Na_2SiO_3$ (0.06g, 0.49mmol) by $GeO_2$(0.06g, 0.56mmol). The pH value is adjusted to about 3.8 with 1.0 M $HNO_3$ and reduced to room temperature with a rate of 10 $^oC$ per hour. The dark green block crystals of **2** are obtained (yield 44% based on Mo). $C_{82}H_{92}Cu_2Ge_2Mo_{24}N_{10}O_{96}$ (5328.54): C 18.87, H 1.70, N 2.68 %. Found: C 18.86 H 1.71, N 2.67 %.

**Synthesis of $[Ni(L_1)_2(L_2)(H_2O)_2(SiMo_{12}O_{40})]\cdot 4H_2O$ (3)**

Complex **3** is synthesized similar to complex **1**, except for the replacement of $CuCl_2\cdot 2H_2O$ (0.1 g, 0.59 mmol) $NiSO_4$(0.1 g, 0.65 mmol) and the pH changes to 3.8 with 1.0 M $HNO_3$. The temperature was reduced to room temperature with a rate of 10 $^oC$ per hour, the green block crystals of **3** are obtained (yield 43% based on Mo). $C_{46}H_{50}Mo_{12}N_6NiO_{48}Si$ (2692.98): C 20.52, H 1.87, N 3.12 %. Found: C 20.53 H 1.89, N 3.10 %.

**Synthesis of $(HL_1)_4(SiMo_{12}O_{40})_2\cdot 3H_2O$ (4)**

Complex **4** is synthesized similar to complex **1**, except that the pH is changed to 2.8. The temperature is reduced to room temperature with a rate of 10 $^oC$ per hour, the yellow block crystals of **2** are obtained (yield 43% based on Mo). $C_{72}H_{70}Mo_{24}N_8O_{87}Si_2$ (4798.10): C 20.52, H 1.87, N 3.12 %. Found: C 20.51 H 1.86, N 3.13 %.

**Synthesis of $(HL_1)_4(GeMo_{12}O_{40})_2\cdot 3H_2O$ (5)**

Complex **5** is synthesized similar to complex **2**, except that the pH is changed to 2.8. The temperature is reduced to room temperature with a rate of 10 $^oC$ per hour, the

yellow block crystals of **5** are obtained (yield 43% based on Mo). $C_{72}H_{70}Mo_{24}N_8O_{87}Ge_2$ (4887.14): C 20.52, H 1.87, N 3.12 %. Found: C 20.53 H 1.88, N 3.11 %.

**Preparation of the Modified Electrodes**

**Preparations of $SiMo_{12}$@TBAB**

A solution of 0.2 mmol of $H_4SiMo_{12}O_{40}$ dissolving in 40 mL of distilled water is added to the solution of 10 mL of distilled water containing 0.48 mmol of tetrabutylammonium bromide (TBAB) under stirring. A resulting turbid suspension is filtrated, and the precipitate is collected, washed with distilled water three times, and dries in the oven at room temperature, then **$SiMo_{12}$@TBAB** can be obtained. The mass loading of active materials for n-GCEs are 16.67 μg.

**Preparation of working electrode**

Before each working electrode preparation, the glass carbon electrode is polished on the antelope skin with 1, 0.3, 0.05 nm $Al_2O_3$ powder before each test, washing with deionized water after each polishing, and sonicated with anhydrous $C_2H_5OH$. Grinding complex **1** (10 mg) with varying amounts of acetylene black for mass ratios of 2:1, 1.5:1, 1:1, 1:1.5, 1:2, 1:2.5 and the complexes **2** – **5** 10 mg with 20 mg mass ratio 1:2 acetylene black for 1 h, get the crystal and acetylene black mixture, weigh 5 mg mixture, add 5 μL 5% Nafion solution, 165 μL $CH_3CH_2OH$ and 330 μL $H_2O$, and sonicate 30 min to form the suspension. 5 μL of suspension is fed onto the polished glass carbon electrode surface and dry at room temperature. Glass-carbon electrodes (**1**– to **5**–GCEs) of complexes **1** – **5** and **$SiMo_{12}$@TBAB** are obtained.

**Synthesis of 1–based carbon paper electrode (CPE)**

To prepare the working electrode, a mixture of complex **1** and acetylene black in a weight ratio of 1:2 is ground in a mortar with a little ethyl alcohol and deionized water to make a well dispersed slurry. Then, 1 mL of the slurry was dropped onto the carbon paper surface (1×1 $cm^2$) and dried for 2 hours at room temperature in order to form a uniform thin film. Then, 10 μL of Nafion solution (Aldrich) was dropped onto the carbon paper surface and the electrode was dried at room temperature.

**Assembly of 1//AC ASC device**

The ASC device was prepared by using **1**–based CPE (1 mg) as negative electrode and

activated carbon (**AC**) as the positive one. The **AC** electrode was prepared by pressing a homogeneous paste of 80 % (wt.) active material (3 mg), 10 % (wt.) carbon black and 10 % (wt.) polyvinylidene fluoride (PVDF) onto carbon paper followed by overnight drying at 60°C. 0.5 M $H_2SO_4$ solutions were used as the electrolyte, and a porous filter paper as the separator.

# Supplementary Figures and Tables

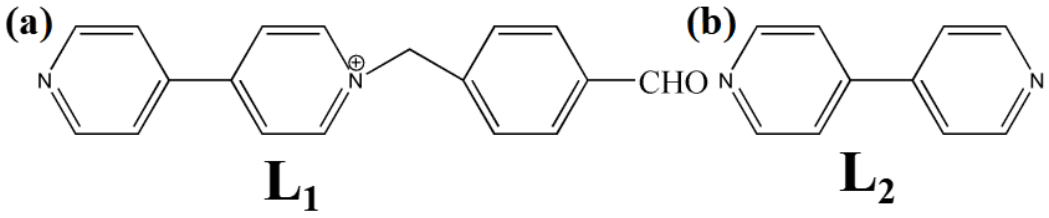


**Scheme S1** The ligands $L_1$ and $L_2$ used in this work.

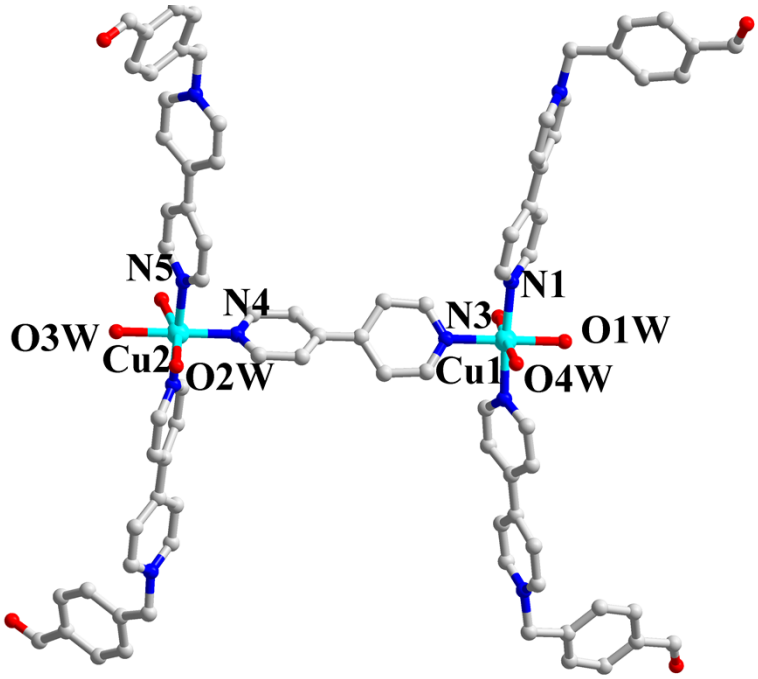


**Fig. S1** (a) The $\{Cu_2(L_1)_4(L_2)(H_2O)_4\}^{4+}$ subunit.

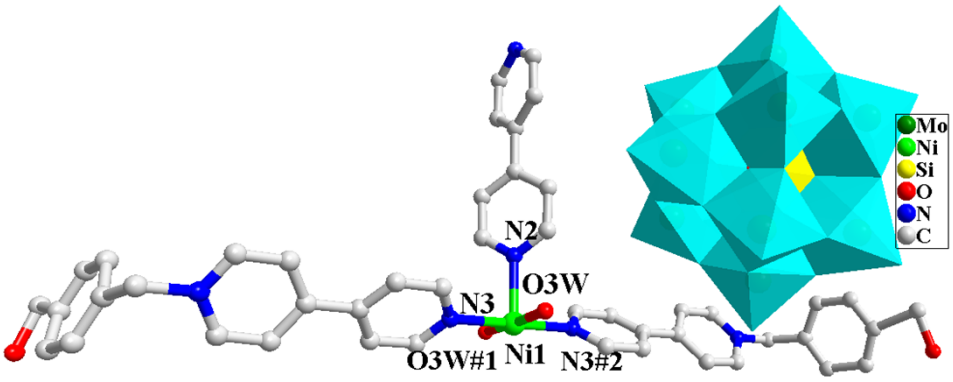


**Fig. S2** Structural unit plot of complex **3**.

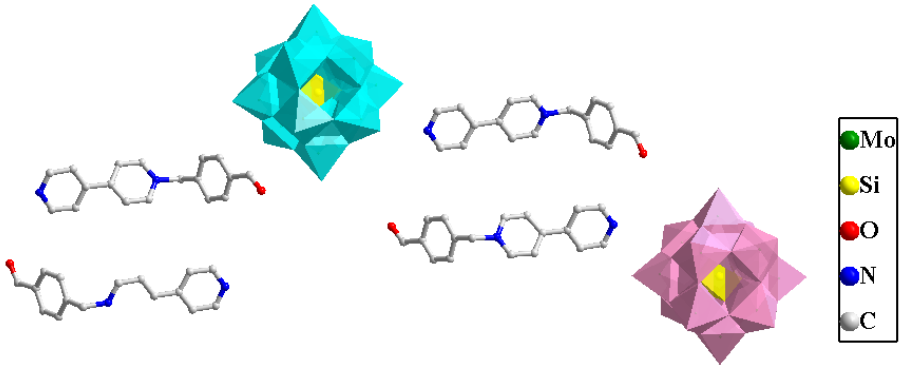


**Fig. S3** Structural unit plot of complex **4**.

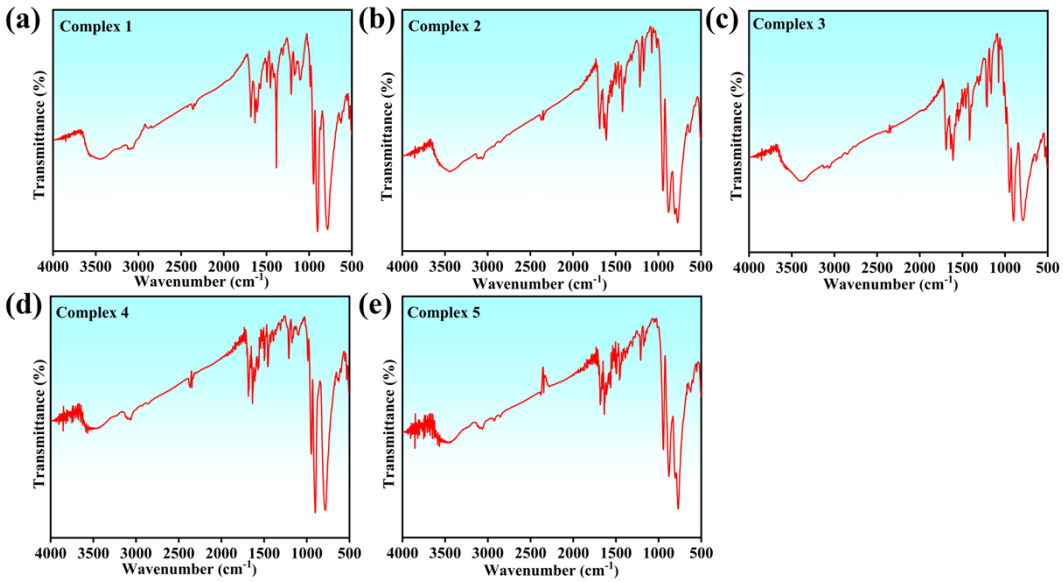


**Fig. S4** (a)-(e) The FTIR spectra of complexes **1** – **5**.

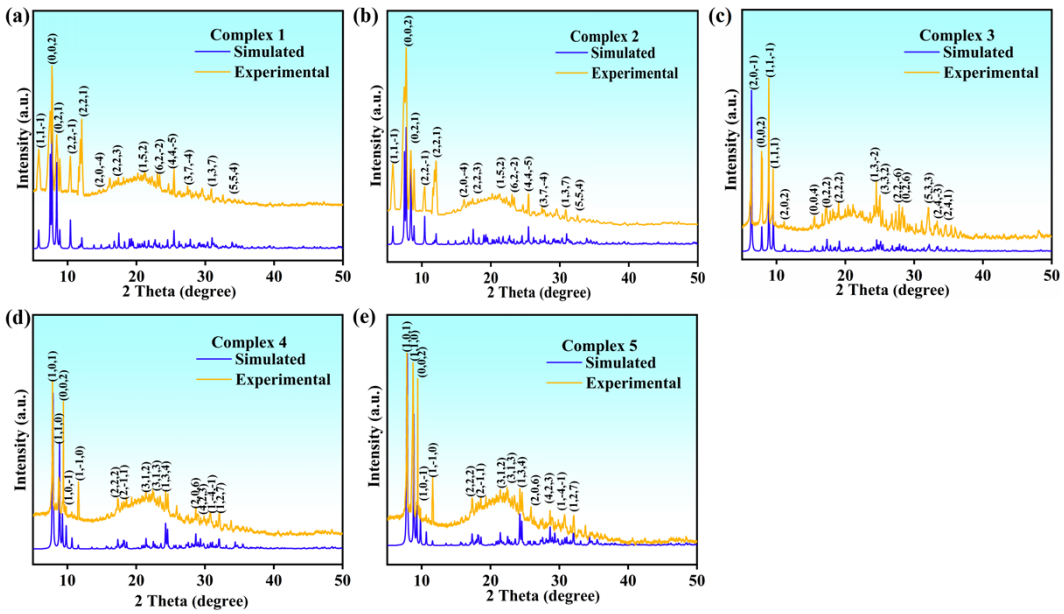


**Fig. S5** (a)-(e) The PXRD patterns of the complexes **1** – **5.**

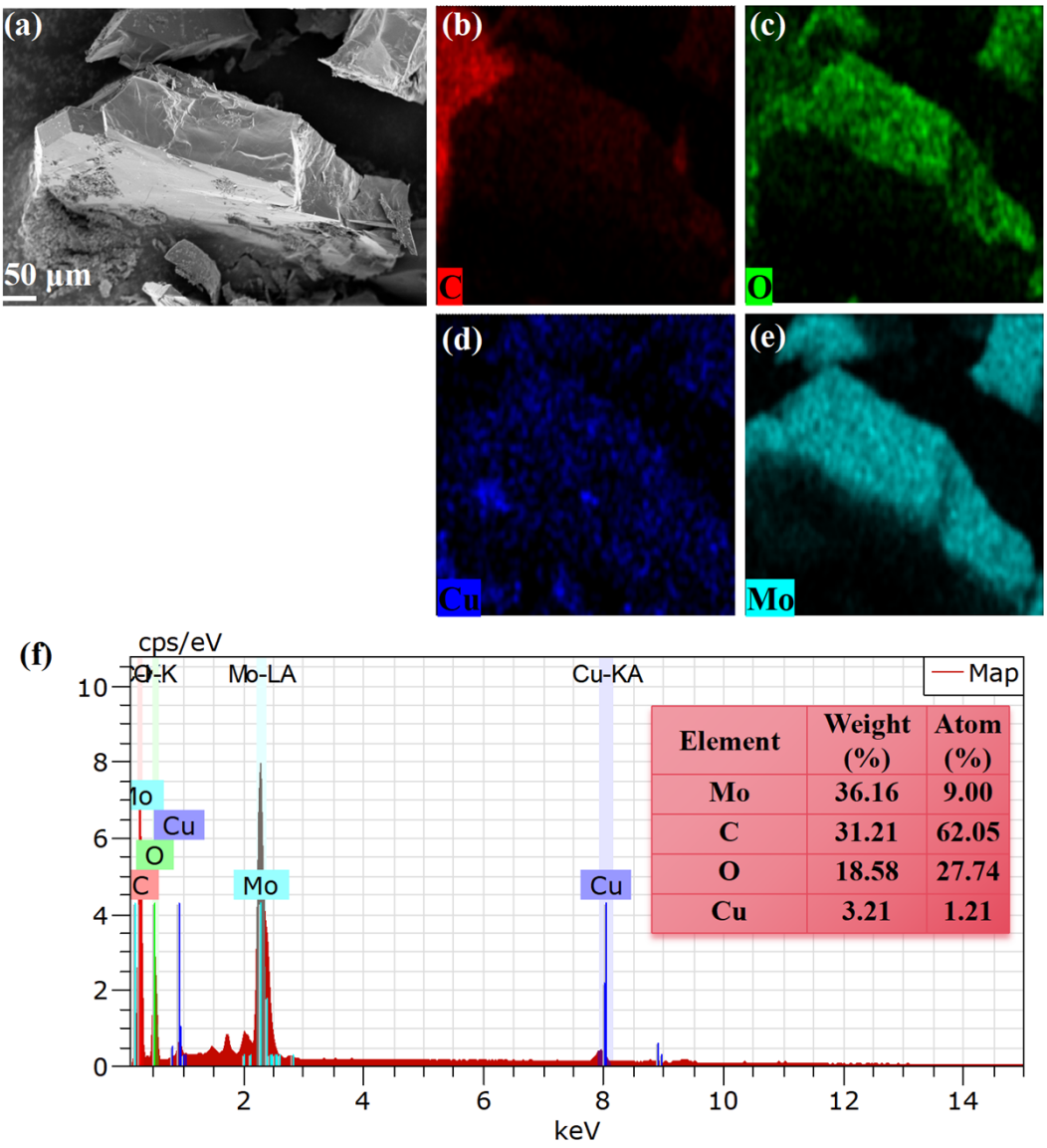


**Fig. S6** (a) The SEM image of complex **1**. (b)-(e) The EDS elemental mapping images of (b) C, (c) O, (d) Cu and (e) Mo. (f) EDS spectrum of complex **1**.

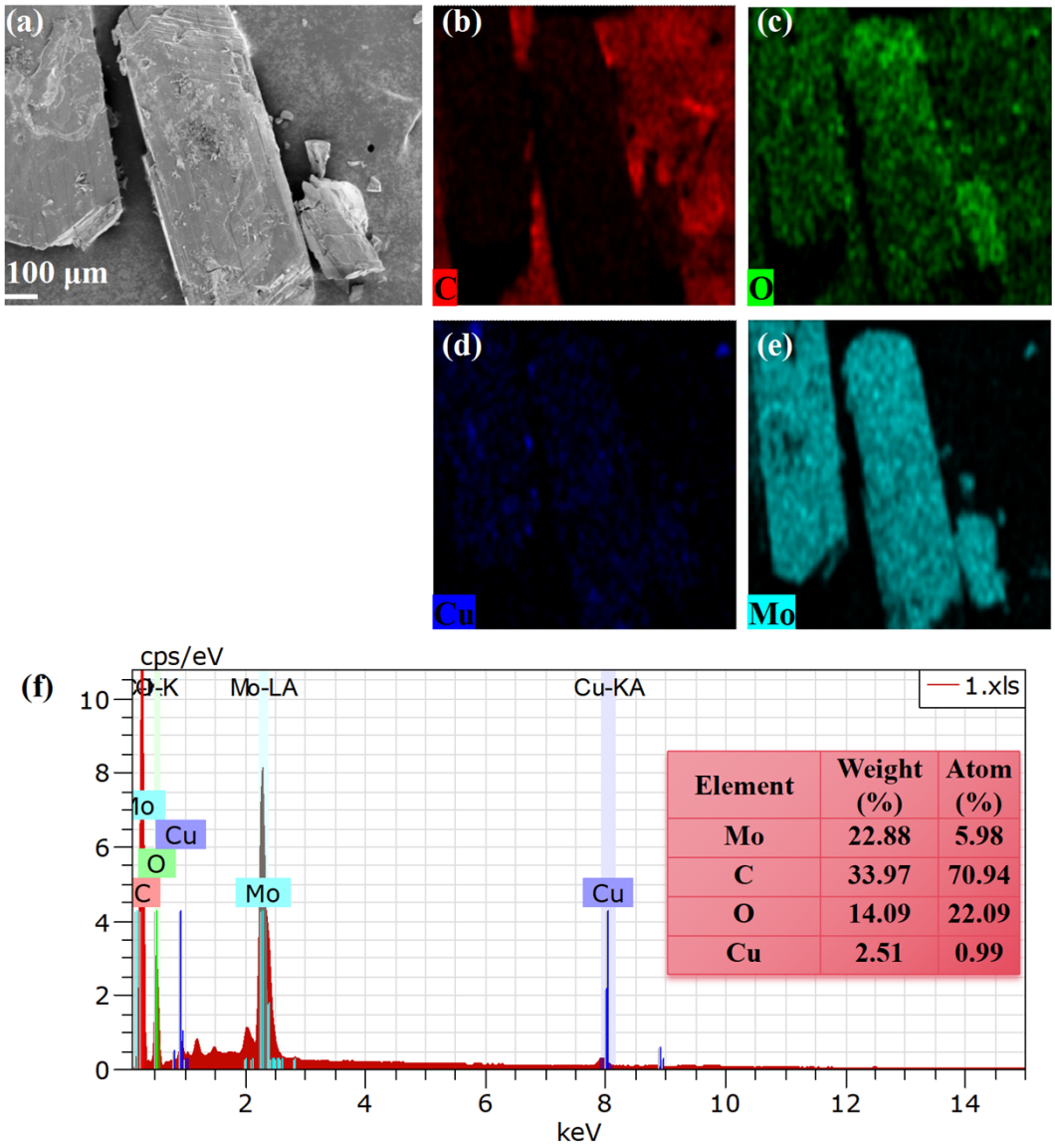


**Fig. S7** The SEM image of complex **2**. (b)-(e) The EDS elemental mapping images of (b) C, (c) O, (d) Cu and (e) Mo. (f) EDS spectrum of complex **2**.

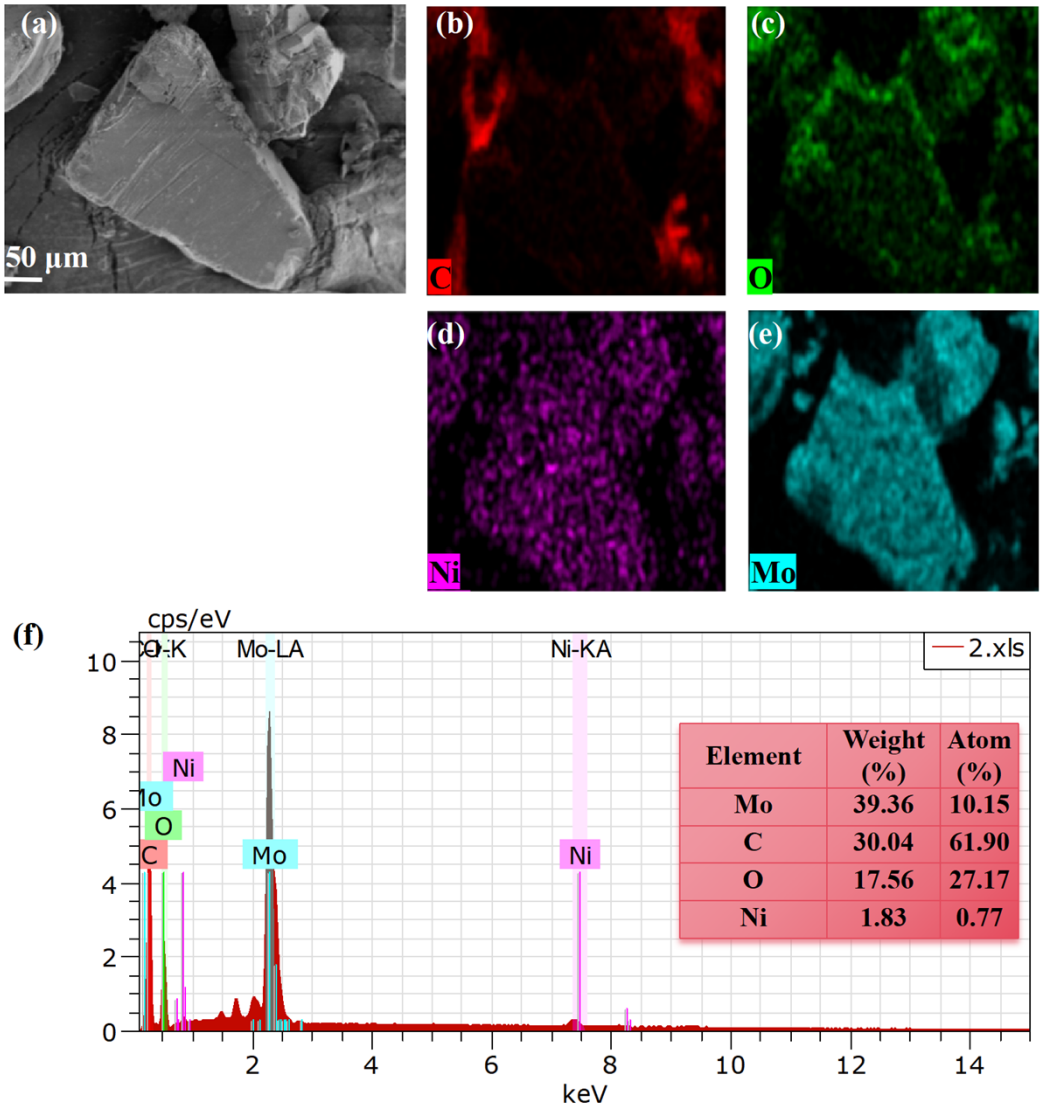


**Fig. S8** The SEM image of complex **3**. (b)-(e) The EDS elemental mapping images of (b) C, (c) O, (d) Ni and (e) Mo. (f) EDS spectrum of complex **3**.

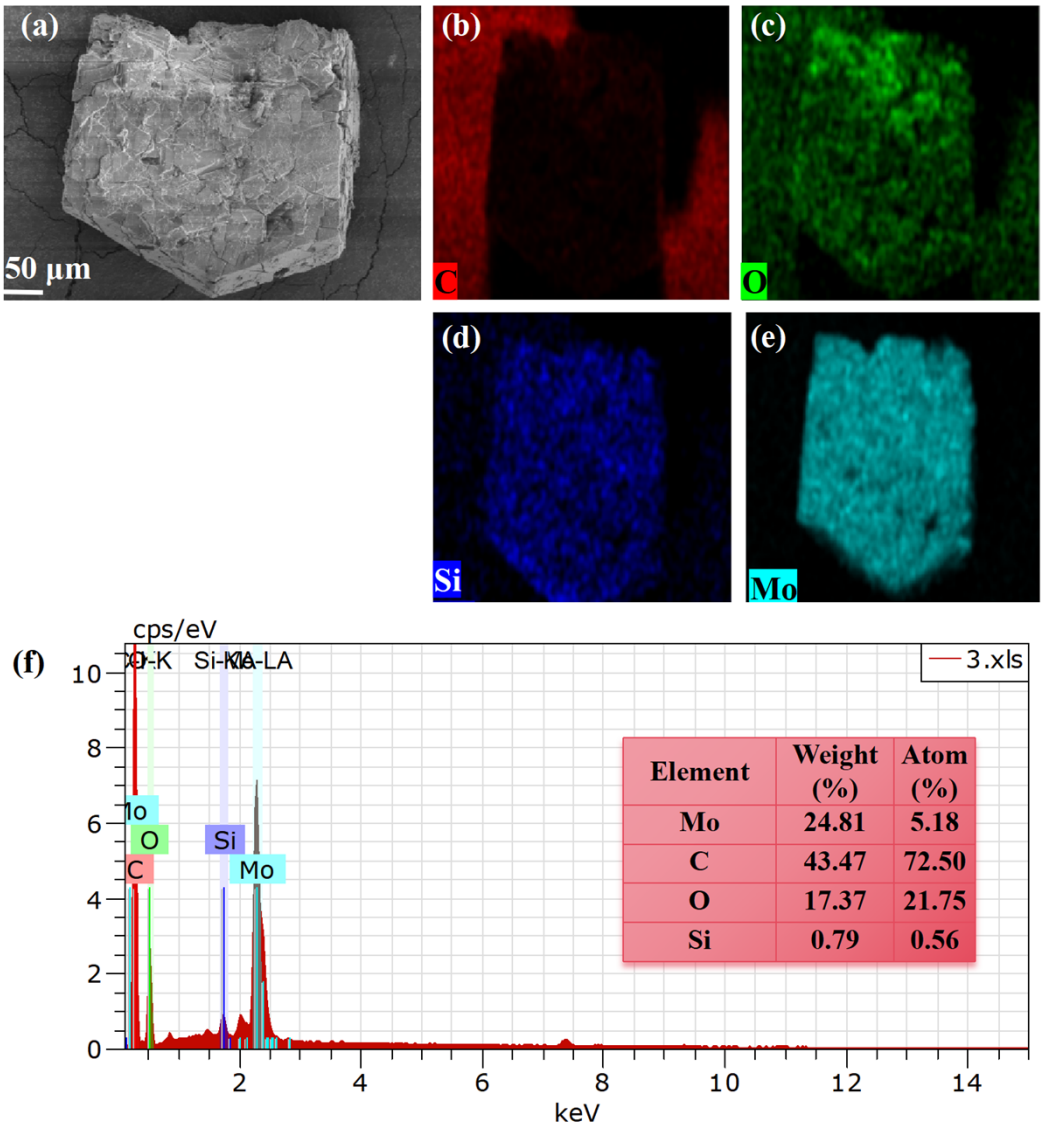


**Fig. S9** The SEM image of complex **4**. (b)-(e) The EDS elemental mapping images of (b) C, (c) O, (d) Si and (e) Mo. (f) EDS spectrum of complex **4**.

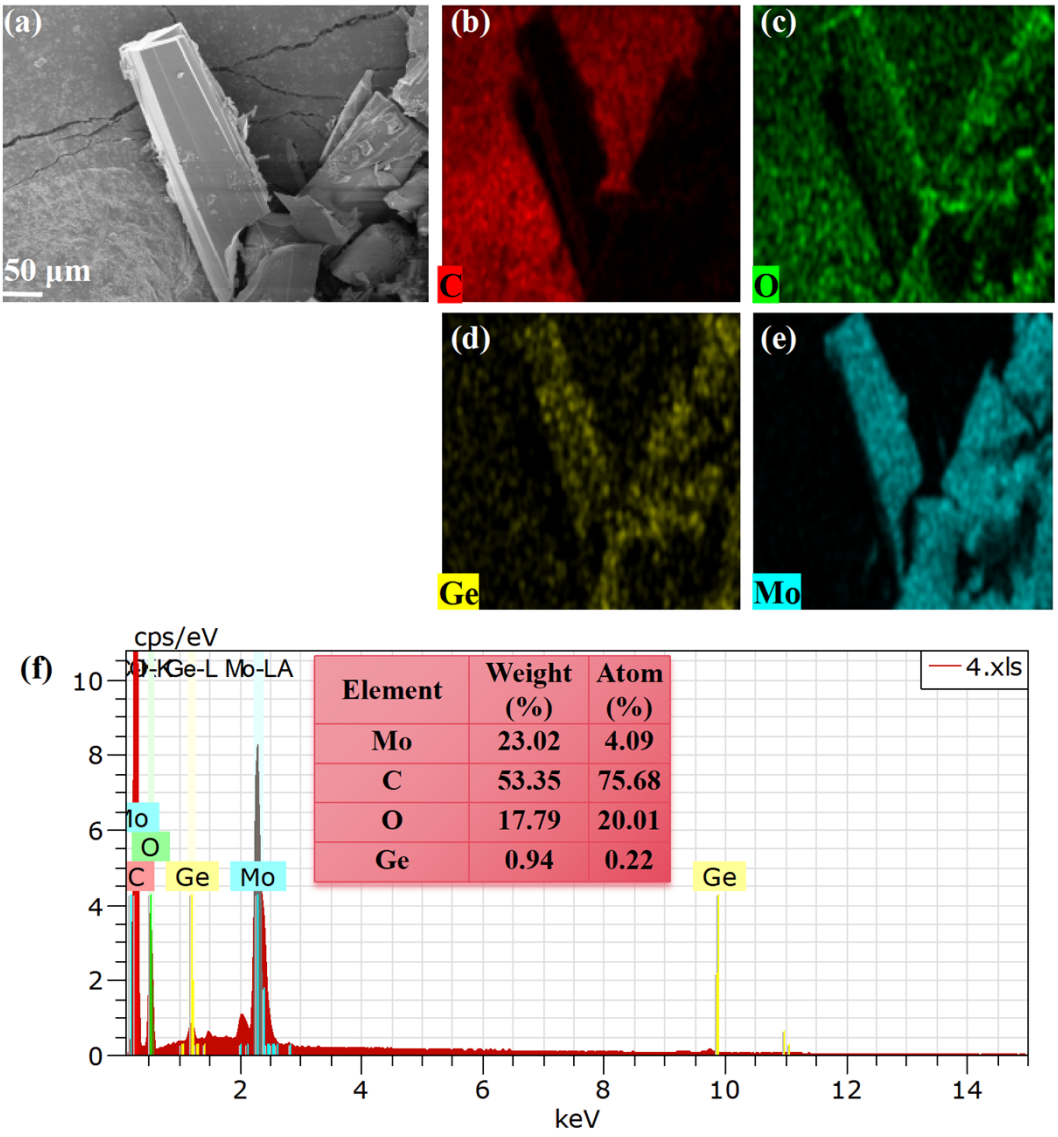


**Fig. S10** The SEM image of complex **5**. (b)-(e) The EDS elemental mapping images of (b) C, (c) O, (d) Ge and (e) Mo. (f) EDS spectrum of complex **5**.

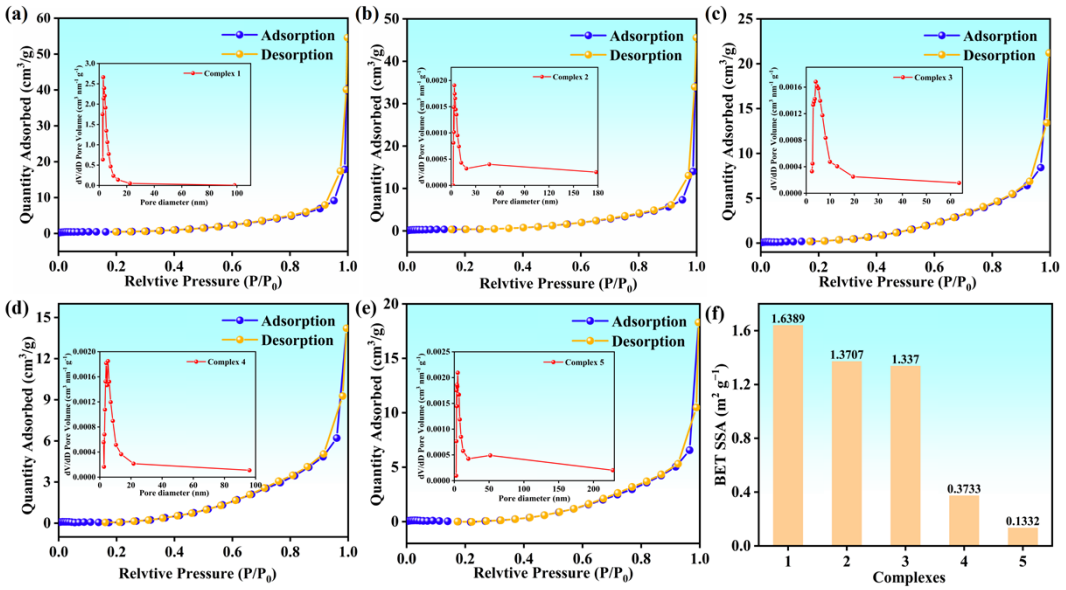


**Fig. S11** (a)-(e) $N_2$ adsorption−desorption isotherms (inset: pore size distribution) and (f) BET SSAs of complexes **1** – **5**.

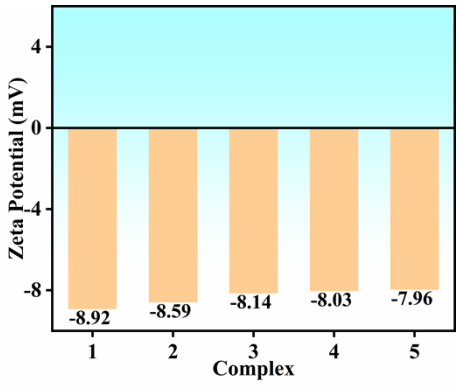


**Fig. S12** The zeta potential of complexes **1** – **5.**

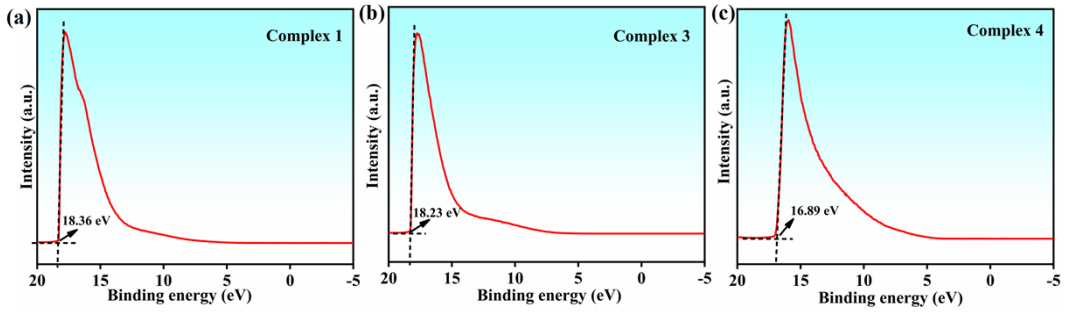


**Fig. S13** (a)-(c) High energy cut-off of UPS spectra recorded for complex **1**, **3** and **4**.

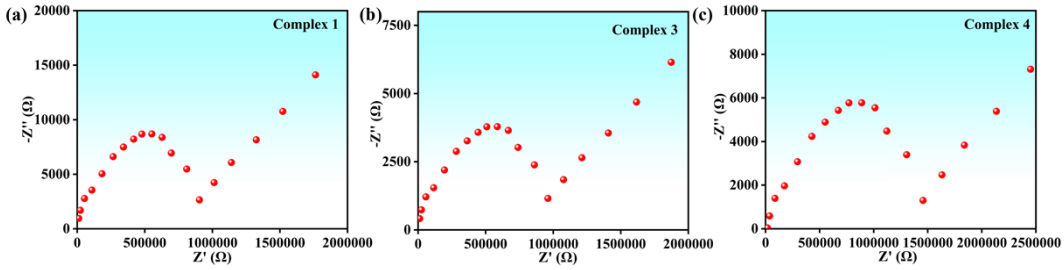


**Fig. S14** (a)-(c) Alternating current impedance plots of complexes **1**, **3** and **4** at room temperature.

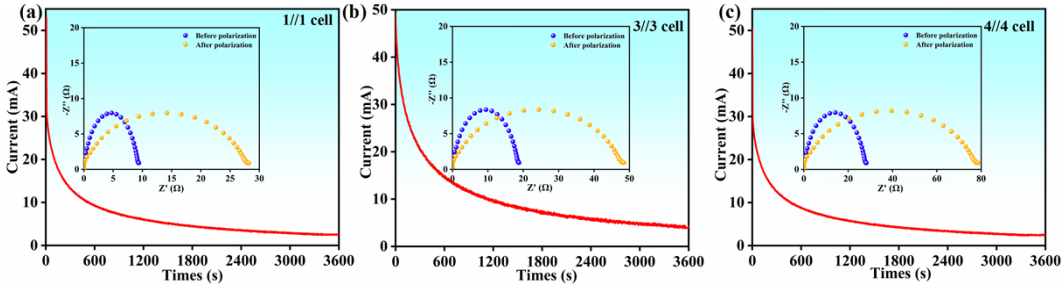


**Fig. S15** (a)-(c) Current-time plots of complexes **1**, **3** and **4** symmetric cells.

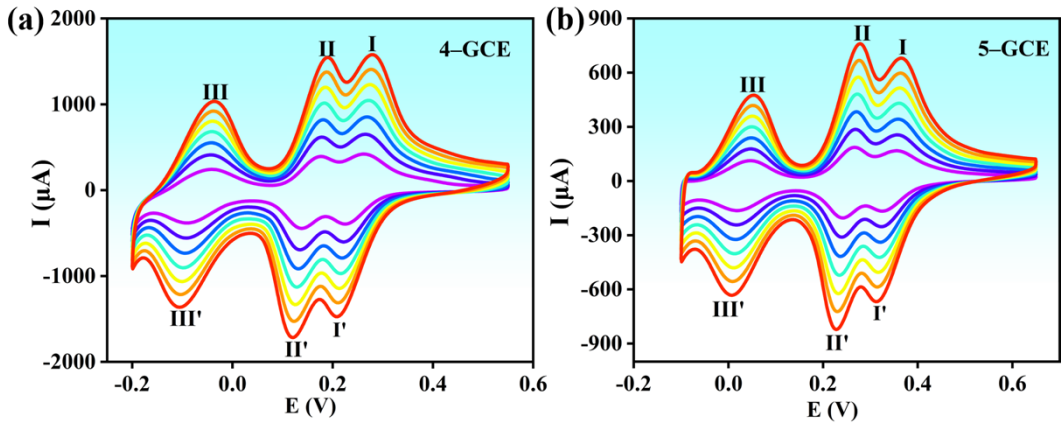


**Fig. S16** (a)-(b) CV curves of **4**– and **5**–GCEs in 0.5 M $H_2SO_4$ aqueous solution at different scan rates (50 to 200 mV $s^{-1}$, respectively).

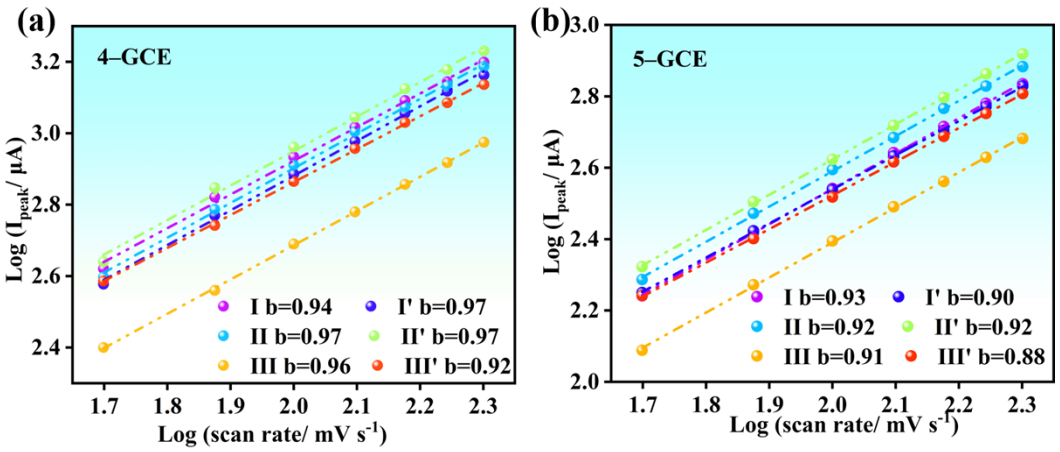


**Fig. S17** (a)-(b) The b values of **4**– and **5**–GCEs.

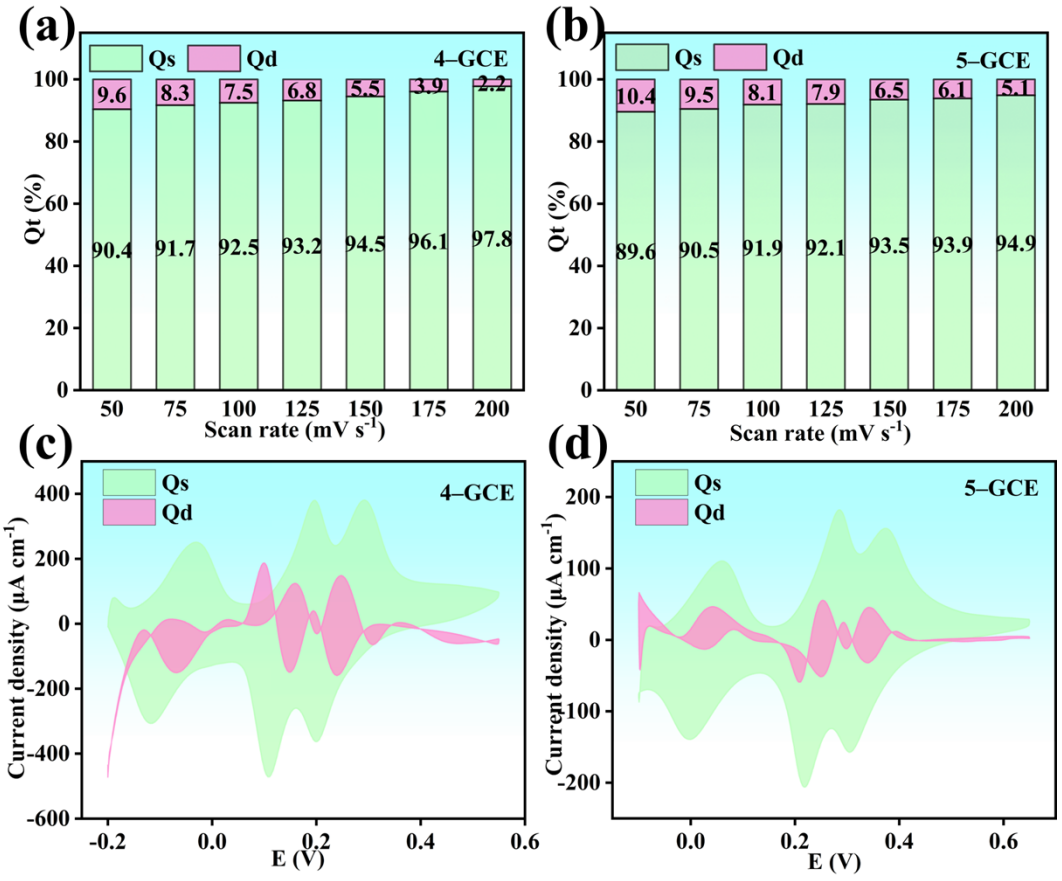


**Fig. S18** (a)-(b) The capacitive (Qs) and diffusion-controlled contribution (Qd) of the **4**– and **5**–GCEs and (c)-(d) the representative CV curves of **4**– and **5**–GCEs.

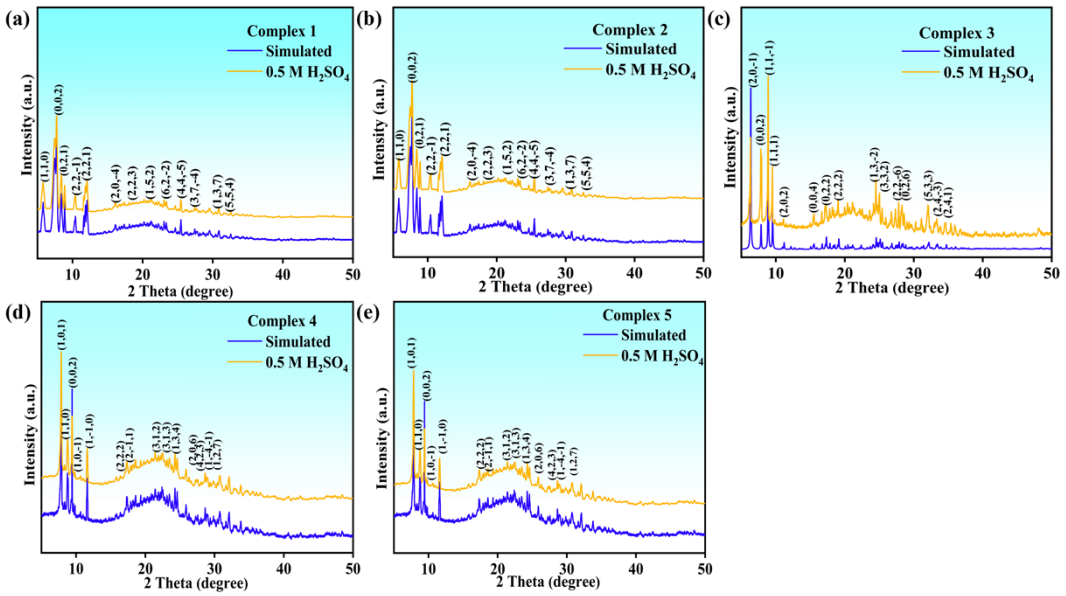


**Fig. S19** (a)-(e) PXRD patterns of complexes **1** – **5** in 0.5 M $H_2SO_4$ solutions more than 48 h.

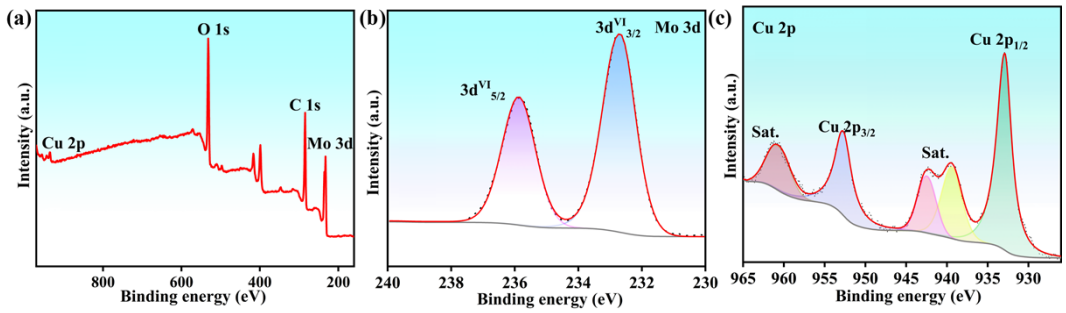


**Fig. S20** The XPS of complex **1** after GCD measurement. (a) XPS survey spectra. High-resolution XPS spectra of (b) Mo 3d and (c) Cu 2p.

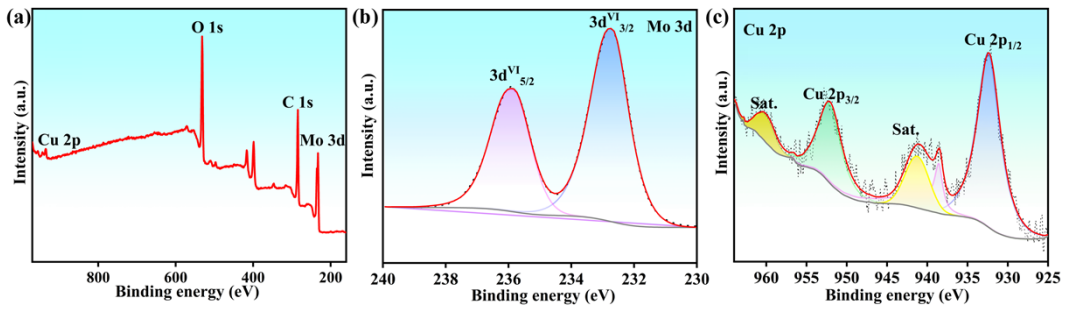


**Fig. S21** The XPS of complex **2** after GCD measurement. (a) XPS survey spectra. High-resolution XPS spectra of (b) Mo 3d and (c) Cu 2p.

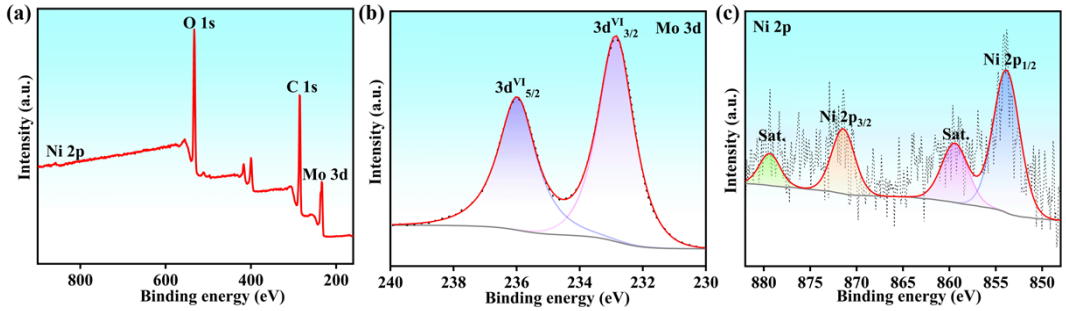


**Fig. S22** The XPS of complex **3** after GCD measurement. (a) XPS survey spectra. High-resolution XPS spectra of (b) Mo 3d and (c) Ni 2p.

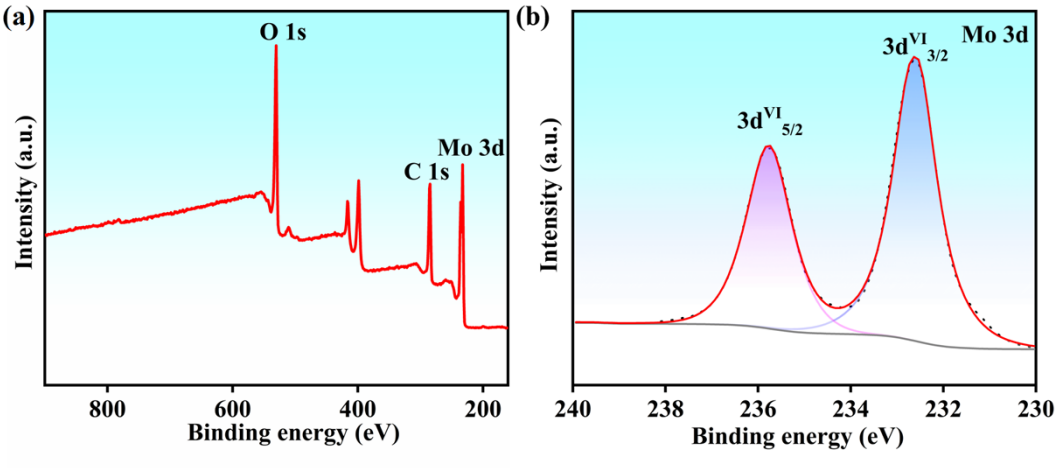


**Fig. S23** The XPS of complex **4** after GCD measurement. (a) XPS survey spectra. (b) High-resolution XPS spectra of Mo 3d.

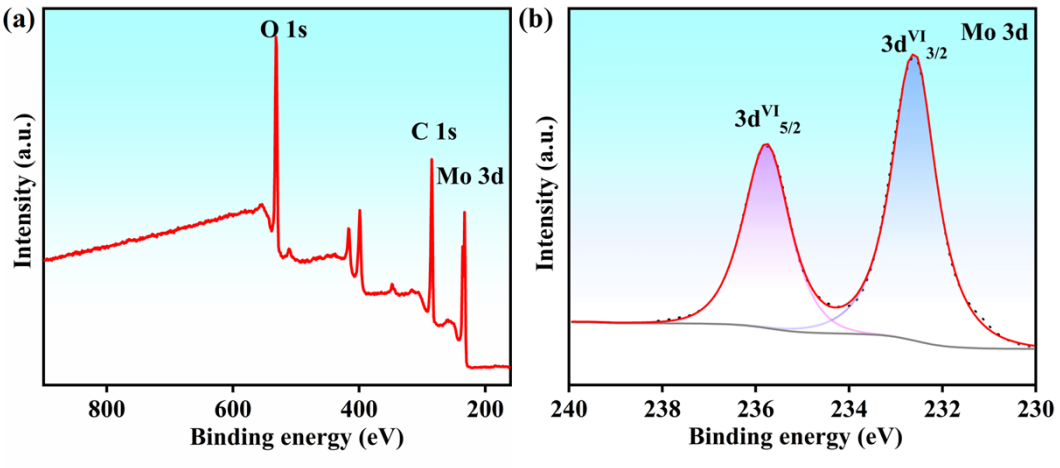


**Fig. S24** The XPS of complex **5** after GCD measurement. (a) XPS survey spectra. (b) High-resolution XPS spectra of Mo 3d.

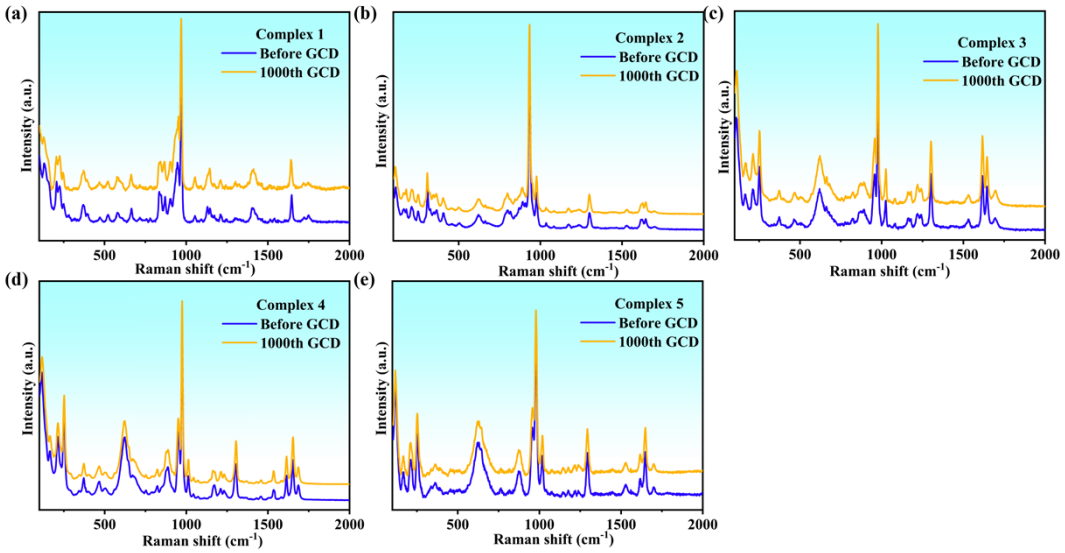


**Fig. S25** (a)-(e) The Raman spectroscopy of complexes **1** – **5** after GCD measurement.

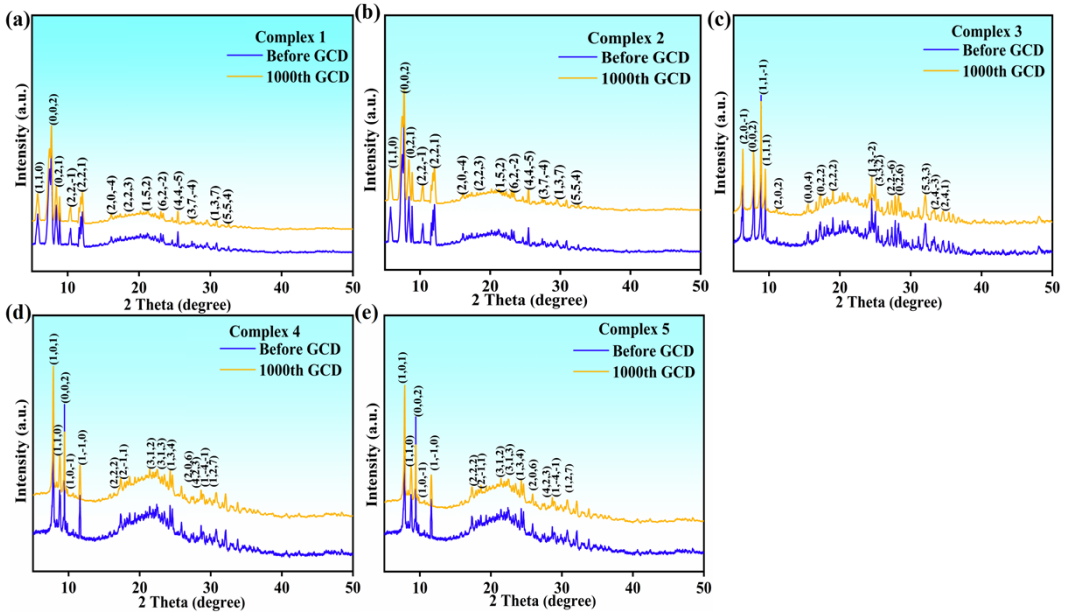


**Fig. S26** (a)-(e) The PXRD of complexes **1** – **5** after GCD measurement.

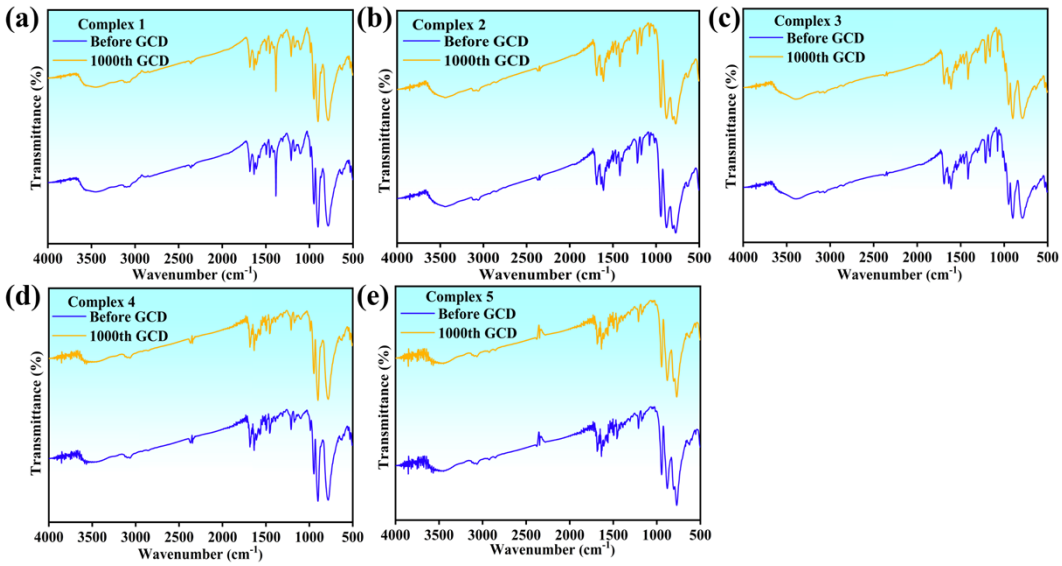


**Fig. S27** (a)-(e) The FTIR spectra of complexes **1** – **5** after GCD measurement.

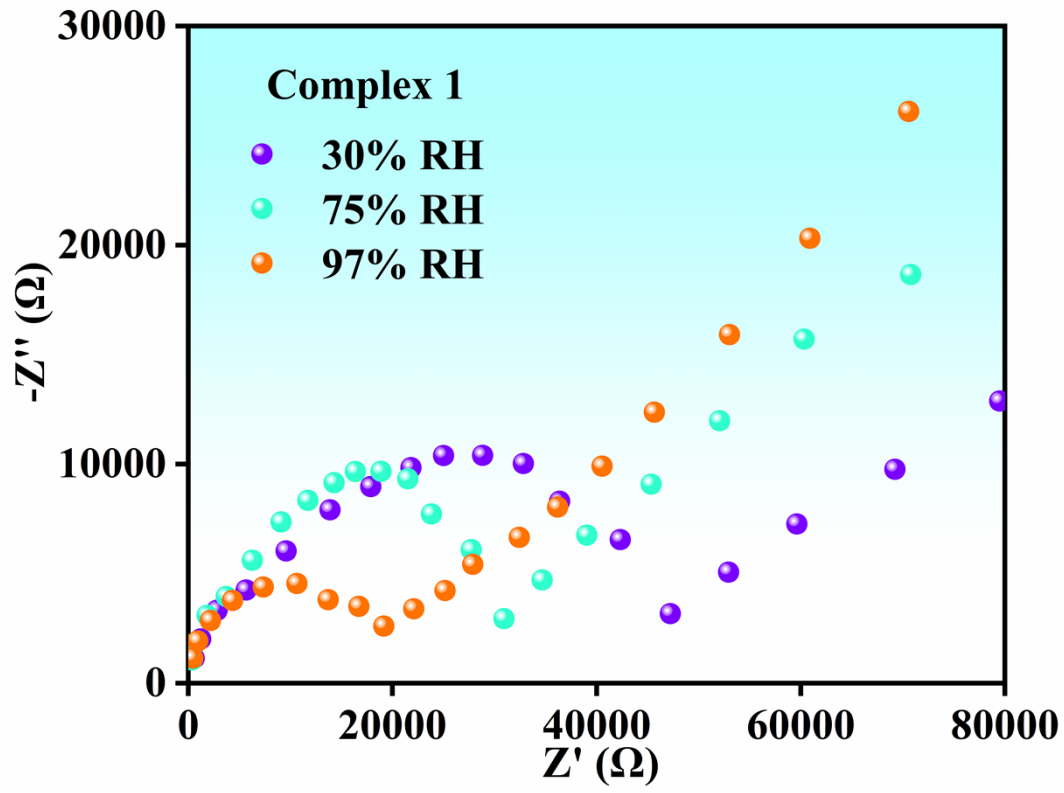


**Fig. S28** Alternating current impedance plots of complex **1** at various RH at 50 °C.

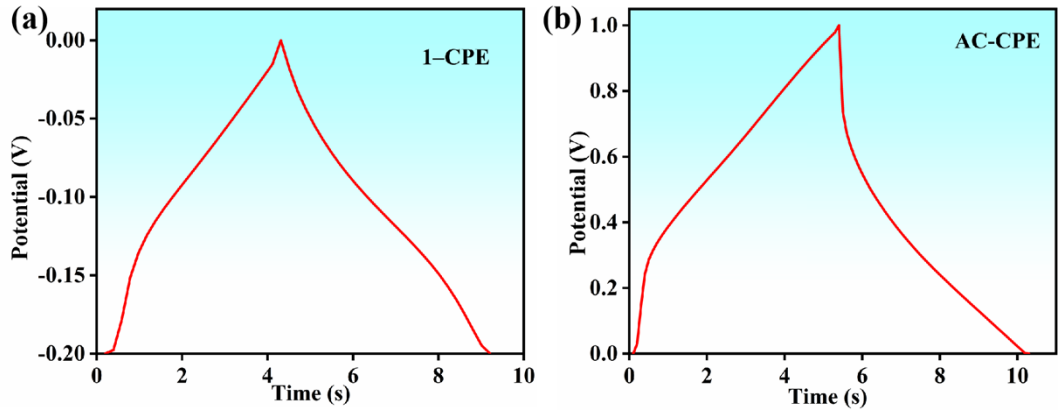


**Fig. S29** The GCD curves at 10 A $g^{-1}$ of (a) **1**–CPE, (b) **AC**–CPE.

**Table S1** Crystal data and structure refinement for complexes **1** – **5**

| | **1** | **2** | **3** | **4** | **5** |
|---|---|---|---|---|---|
| formula | $C_{82}H_{92}Cu_2Si_2Mo_{24}N_{10}O_{96}$ | $C_{82}H_{92}Cu_2Ge_2Mo_{24}N_{10}O_{96}$ | $C_{46}H_{50}Mo_{12}N_6NiO_{48}Si$ | $C_{72}H_{70}Mo_{24}N_8O_{87}Si_2$ | $C_{72}H_{70}Mo_{24}N_8O_{87}Ge_2$ |
| Fw | 5239.50 | 5328.54 | 2692.98 | 4798.10 | 4887.14 |
| Crystal system | monoclinic | monoclinic | monoclinic | triclinic | triclinic |
| Space group | C 2/c | C 2/c | C 2/c | P-1 | P-1 |
| a (Å) | 24.967(3) | 24.9635(10) | 28.576(3) | 12.5280(4) | 12.5426(4) |
| b (Å) | 23.613(3) | 23.6357(10) | 11.4638(11) | 13.4619(4) | 13.4815(4) |
| c (Å) | 24.147(2) | 24.2410(11) | 23.138(2) | 20.0402(5) | 20.0643(6) |
| α (°) | 90 | 90 | 90 | 77.8990(10) | 77.9290(10) |
| β (°) | 108.749(4) | 108.824(2) | 103.444(3) | 73.1450(10) | 73.3260(10) |
| γ (°) | 90 | 90 | 90 | 72.1340(10) | 72.2640(10) |
| V (Å$^3$) | 13480(3) | 13537.9(10) | 7372.1(12) | 3051.48(15) | 3067.94(16) |
| Z | 4 | 4 | 4 | 1 | 1 |
| $D_c$ (g·cm$^{-3}$) | 5.575 | 2.605 | 2.426 | 2.611 | 2.645 |
| μ (mm$^{-1}$) | 2.589 | 2.996 | 2.340 | 2.506 | 2.954 |
| F(000) | 10040.0 | 10160.0 | 5192.0 | 2290.0 | 2326.0 |
| $R_1$[a] [I > 2σ(I)] | 0.0644 | 0.0307 | 0.0761 | 0.0494 | 0.0576 |
| $wR_2$[b] (all data) | 0.1812 | 0.0802 | 0.1804 | 0.1172 | 0.1315 |
| GOF on F$^2$ | 1.095 | 1.030 | 1.053 | 1.083 | 1.086 |

[a] $R_1=\sum \| Fo | - | Fc \| / \sum | Fo |$. [b] $wR_2 = \{\sum[w(Fo^2-Fc^2)^2]/\sum[w(Fo^2)^2]\}^{1/2}$

**Table S2** Selected bond distances (Å) and angles (°) for complexes **1** – **5**

| Complex 1 | | | |
|---|---|---|---|
| **Atoms** | **Distance** | **Atoms** | **Distance** |
| Cu1-O1W | 1.973(15) | Cu1-N1 | 2.036(12) |
| Cu1-N1[1] | 2.036(12) | Cu1-N3 | 2.015(17) |
| Cu2-N5 | 2.026(12) | Cu2-N5[1] | 2.025(13) |
| Cu2-N4 | 2.003(17) | Cu2-O3W | 2.06(2) |
| Cu2-O2W[1] | 2.354(17) | Cu2-O2W | 2.354(17) |
| **Atoms** | **Angle** | **Atoms** | **Angle** |
| O1W-Cu1-N1[1] | 88.0(3) | O1W-Cu1-N1 | 88.0(3) |
| O1W-Cu1-N3 | 180.0 | N1-Cu1-N1[1] | 176.0(6) |
| N3-Cu1-N1 | 92.0(3) | N3-Cu1-N1[1] | 92.0(3) |
| N5[1]-Cu2-N5 | 179.6(7) | N5[1]-Cu2-O3W | 90.2(4) |
| N5-Cu2-O3W | 90.2(4) | N5-Cu2-O2W | 92.8(5) |
| N5[1]-Cu2-O2W | 87.2(5) | N5-Cu2-O2W[1] | 87.2(5) |
| N5[1]-Cu2-O2W[1] | 92.8(5) | N4-Cu2-N5 | 89.8(4) |
| N4-Cu2-N5[1] | 89.8(4) | N4-Cu2-O3W | 180.0 |
| N4-Cu2-O2W[1] | 97.0(4) | N4-Cu2-O2W | 97.0(4) |
| O3W-Cu2-O2W[1] | 83.0(4) | O3W-Cu2-O2W | 83.0(4) |
| O2W-Cu2-O2W[1] | 166.0(9) | | |
| Symmetry codes for **1**: 1-X,+Y,1/2-Z | | | |
| **Complex 2** | | | |
| **Atoms** | **Distance** | **Atoms** | **Distance** |
| Cu1- N1 | 1.983(6) | Cu1-N3[1] | 2.036(5) |
| Cu1-N3 | 2.036(5) | Cu1-O2W | 2.022(7) |
| Cu1-O1W[1] | 2.393(5) | Cu1-O1W | 2.393(5) |
| Cu2-O3W | 1.989(6) | Cu2-N5[1] | 2.018(5) |
| Cu2-N5 | 2.018(5) | Cu2-N2 | 2.011(7) |
| **Atoms** | **Angle** | **Atoms** | **Angle** |
| N1-Cu1-N3 | 89.94(14) | N1-Cu1-N3[1] | 89.94(14) |
| N1-Cu1-O2W | 180 | N1-Cu1-O1W | 96.59(14) |
| N1-Cu1-O1W[1] | 96.59(14) | N3[1]-Cu1-N3 | 179.9(3) |
| N3-Cu1-O1W[1] | 88.90(19) | N3[1]-Cu1-O1W[1] | 91.12(19) |
| N3-Cu1-O1W | 91.12(19) | N3[1]-Cu1-O1W | 88.89(19) |

| | | | |
|---|---|---|---|
| O2W-Cu1-N3 | 90.06(14) | O2W-Cu1-N3[1] | 90.06(14) |
| O2W-Cu1-O1W | 83.41(14) | O2W-Cu1-O1W[1] | 83.42(14) |
| O1W[1]-Cu1-O1W | 166.8(3) | O3W-Cu2-N5[1] | 87.69(13) |
| O3W-Cu2-N5 | 87.69(13) | O3W-Cu2-N2 | 180 |
| N5-Cu2-N5[1] | 175.4(3) | N2-Cu2-N5[1] | 92.31(13) |
| N2-Cu2-N5 | 92.31(13) | | |

Symmetry codes for **2**: 1-X,+Y,3/2-Z

**Complex 3**

| **Atoms** | **Distance** | **Atoms** | **Distance** |
|---|---|---|---|
| Ni1-O3W | 2.074(8) | Ni1-O3W[2] | 2.074(8) |
| Ni1-N2[3] | 2.165(13) | Ni1-N1 | 2.169(14) |
| Ni1-N3 | 2.105(11) | Ni1-N3[2] | 2.105(11) |
| **Atoms** | **Angle** | **Atoms** | **Angle** |
| O3W[2]-Ni1-O3W | 177.2(4) | O3W[2]-Ni1-N2[3] | 88.6(2) |
| O3W-Ni1-N2[3] | 88.6(2) | O3W[2]-Ni1-N1 | 91.4(2) |
| O3W-Ni1-N1 | 91.4(2) | O3W[2]-Ni1-N3[2] | 90.5(4) |
| O3W-Ni1-N3[2] | 89.5(4) | O3W-Ni1-N3 | 89.5(4) |
| N2[3]-Ni1-N1 | 180.0 | N3-Ni1-N2[3] | 90.1(3) |
| N3[2]-Ni1-N2[3] | 90.1(3) | N3-Ni1-N1 | 89.9(3) |
| N3[2]-Ni1-N1 | 89.9(3) | N3-Ni1-N3[2] | 179.9(5) |

Symmetry codes for **3**: [1]3/2-X,3/2-Y,2-Z; [2]1-X,+Y,3/2-Z; [3]+X,1+Y,+Z;[4]+X,-1+Y,+Z

**Complex 4**

| **Atoms** | **Distance** | **Atoms** | **Distance** |
|---|---|---|---|
| Si1-O1[2] | 1.516(9) | Si2-O21[1] | 1.503(9) |
| Si1-O1 | 1.516(9) | Si2-O21 | 1.503(9) |
| Si1-O2 | 1.698(9) | Si2-O22 | 1.744(9) |
| Si1-O2[2] | 1.698(9) | Si2-O22[1] | 1.744(9) |
| Mo5-O8 | 1.994(6) | Mo5-O6 | 2.025(13) |
| Mo5-O9 | 1.814(6) | Mo5-O1 | 2.418(9) |
| Mo5-O18 | 1.659(6) | Mo7-O23 | 1.969(6) |
| Mo5-O7 | 1.766(11) | Mo7-O24 | 1.806(6) |
| **Atoms** | **Angle** | **Atoms** | **Angle** |
| O8-Mo5-O6 | 83.8(4) | O18-Mo5-O6 | 86.5(5) |

| | | | |
|---|---|---|---|
| O8-Mo5-O1 | 63.8(3) | O18-Mo5-O1 | 159.5(4) |
| O9-Mo5-O8 | 88.1(3) | O7-Mo5-O8 | 145.8(5) |
| O9-Mo5-O6 | 169.3(5) | O7-Mo5-O9 | 93.9(4) |
| O9-Mo5-O1 | 68.2(3) | O7-Mo5-O6 | 88.8(5) |
| O18-Mo5-O8 | 99.1(3) | O7-Mo5-O1 | 85.3(5) |
| O18-Mo5-O9 | 101.8(4) | O6-Mo5-O1 | 101.8(5) |
| O18-Mo5-O7 | 113.8(5) | O23-Mo7-O32 | 81.9(3) |

Symmetry codes for: [1]2-X, -Y,1-Z; [2]1-X,1-Y,-Z

**Complex 5**

| **Atoms** | **Distance** | **Atoms** | **Distance** |
|---|---|---|---|
| Mo1-O29 | 2.004(8) | Mo4-O17 | 1.644(7) |
| Mo1-O25 | 1.811(7) | Mo4-O1 | 2.266(11) |
| Mo1-O30 | 1.654(7) | Mo4-O12[2] | 1.990(8) |
| Mo1-O36[1] | 2.003(8) | Mo4-O16 | 1.837(9) |
| Mo1-O22[1] | 2.240(11) | Mo6-O4 | 1.989(7) |
| Mo1-O26 | 1.912(13) | Mo6-O6 | 1.792(8) |
| Mo4-O5 | 1.972(7) | Mo6-O15 | 1.652(8) |
| Mo4-O4 | 1.802(7) | Mo6-O3 | 1.939(14) |
| **Atoms** | **Angle** | **Atoms** | **Angle** |
| O29-Mo1-O22[1] | 93.7(4) | O30-Mo1-O22[1] | 154.0(5) |
| O25-Mo1-O29 | 88.1(3) | O30-Mo1-O26 | 89.9(6) |
| O25-Mo1-O36[1] | 157.6(5) | O36[1]-Mo1-O29 | 79.3(4) |
| O25-Mo1-O22[1] | 100.2(4) | O36[1]-Mo1-O22[1] | 62.7(5) |
| O25-Mo1-O26 | 101.1(5) | O26-Mo1-O29 | 165.8(5) |
| O30-Mo1-O29 | 98.7(4) | O26-Mo1-O36[1] | 88.5(5) |
| O30-Mo1-O25 | 102.9(5) | O26-Mo1-O22[1] | 74.1(6) |
| O30-Mo1-O36[1] | 97.2(6) | O5-Mo4-O1 | 92.5(4) |

Symmetry codes for : [1]3-X,-1-Y,2-Z; [2]2-X,-Y,1-Z

**Table S3** Some weak interactions (Å) in the structures including convenient H-bonds

| Complex 1 | | | | |
|---|---|---|---|---|
| **D-H···A** | **D-H** | **H-A** | **D···A** | **Angle** |
| O2W-H2WA···O7W | 0.85 | 1.86 | 2.71 | 180 |
| O7W-H7WA···O15 | 0.85 | 2.22 | 2.78 | 125 |
| O5W-H5WA···O33 | 0.85 | 2.33 | 2.87 | 121 |
| O5W-H5WB···O22 | 0.85 | 2.18 | 2.87 | 137 |
| O1W-H1WB···O5W | 0.85 | 1.92 | 2.76 | 168 |
| O1W-H1WA···O5W | 0.85 | 1.91 | 2.76 | 179 |
| C11-H11A···O42 | 0.93 | 2.49 | 3.10 | 121 |
| O8W-H8WB···O35 | 0.85 | 2.49 | 3.03 | 122 |
| O6W-H6WB···O8W | 0.85 | 1.98 | 2.51 | 119 |
| O6W-H6WB···O5W | 0.85 | 2.56 | 3.25 | 139 |
| **Complex 3** | | | | |
| **D-H···A** | **D-H** | **H-A** | **D···A** | **Angle** |
| O3W-H3WB···O1W | 0.99 | 2.04 | 2.63 | 116 |
| O3W-H3WA···O1W | 1.00 | 2.16 | 2.63 | 107 |
| O2W-H2WA···O1W | 0.85 | 1.76 | 2.61 | 180 |
| O2W-H2WB···O3 | 0.85 | 2.63 | 2.64 | 95 |
| O2W-H2WB···O15 | 0.85 | 2.28 | 3.02 | 145 |
| O3W-H3WB···O21 | 0.99 | 2.57 | 3.06 | 102 |
| C13-H13···O7 | 0.93 | 2.95 | 3.10 | 91 |
| **Complex 4** | | | | |
| **D-H···A** | **D-H** | **H-A** | **D···A** | **Angle** |
| O1W-H1WB···O2W | 0.85 | 1.73 | 2.58 | 175 |
| O3W-H3WA···O32 | 0.80 | 2.36 | 2.84 | 119 |
| O3W-H3WB···O42 | 0.85 | 2.02 | 2.76 | 144 |
| O1W-H1WA···O15 | 0.85 | 3.01 | 3.04 | 95 |
| N3-H3···O2W | 0.86 | 2.26 | 2.87 | 128 |
| O1W-H1WA···O41 | 0.85 | 1.66 | 2.51 | 179 |
| N1-H1···O3W | 0.86 | 2.17 | 2.84 | 134 |

**Table S4** Pore Size distribution of complexes **1** – **5**.

| Complexes | pore size (nm) |
|---|---|
| **1** | 2.97 |
| **2** | 3.52 |
| **3** | 3.99 |
| **4** | 5.21 |
| **5** | 5.67 |

**Table S5** The Specific Capacitance of complex **1** at various mass ratios

| | **2:1** | **1.5:1** | **1:1** | **1:1.5** | **1:2** | **1:2.5** |
|---|---|---|---|---|---|---|
| 2 A $g^{-1}$ | 576.6 | 600.6 | 924.8 | 1516.2 | 1618.4 | 675.2 |
| 5 A $g^{-1}$ | 350.6 | 360 | 616 | 1065.4 | 1398 | 552 |
| 10 A $g^{-1}$ | 272 | 309.4 | 522.6 | 914.6 | 1287.3 | 488 |
| 15 A $g^{-1}$ | 240 | 285.4 | 488 | 852 | 1199.5 | 456 |
| 20 A $g^{-1}$ | 224 | 270 | 466 | 816 | 1164.2 | 442.6 |

**Table S6** Specific Capacitance of Complexes **1** – **5**

| | **1** | **2** | **3** | **4** | **5** |
|---|---|---|---|---|---|
| 2 A $g^{-1}$ | 1618.4 | 1457.6 | 1421.6 | 1208.7 | 704 |
| 5 A $g^{-1}$ | 1398 | 1311.3 | 1270 | 821.7 | 602.6 |
| 10 A $g^{-1}$ | 1287.3 | 1241.3 | 1141.3 | 620 | 550.7 |
| 15 A $g^{-1}$ | 1199.5 | 1178 | 1012 | 579.3 | 528 |
| 20 A $g^{-1}$ | 1164.2 | 1157.3 | 938.7 | 523.3 | 512 |

**Table S7.** Comparision of the specific capacitance values between complexes in this

work and reported POMs-based electrode materials.

| | Electrode material | Electrolyte | Scan rate/Current density | Specific capacitance | **Ref.** |
|---|---|---|---|---|---|
| 1 | $Zn_2(DEP)_2(H_2O)_6[H_2(TeMo_6O_{24})]$ | 0.1 M $H_2SO_4$ + 0.5 M $Na_2SO_4$ | 1 A $g^{-1}$ | 412.77 F $g^{-1}$ | **4** |
| 2 | $\{Co(DEP)_2(H_2O)_2[H_2(\gamma\text{-}Mo_8O_{26})]\}\cdot 11H_2O$ | 0.1 M $H_2SO_4$ + 0.5 M $Na_2SO_4$ | 1 A $g^{-1}$ | 580 F $g^{-1}$ | |
| 3 | $Cu(DEP)\ [(H_2\beta\text{-}Mo_8O_{26})_{0.5}]$ | 0.1 M $H_2SO_4$ + 0.5 M $Na_2SO_4$ | 1 A $g^{-1}$ | 823.09 F $g^{-1}$ | |
| 4 | $[H(C_{10}H_{10}N_2)Cu_2][PMo_{12}O_{40}]$ | 0.5 M $H_2SO_4$ | 1 A $g^{-1}$ | 287 F $g^{-1}$ | **5** |
| 5 | $[H(C_{10}H_{10}N_2)Cu_2][PW_{12}O_{40}]$ | 0.5 M $H_2SO_4$ | 1 A $g^{-1}$ | 153.4 F $g^{-1}$ | |
| 6 | $[Cu^{I}H_2(C_{12}H_{12}N_6)(PMo_{12}O_{40})].[(C_6H_{15}N)(H_2O)_2]$ | 1 M $H_2SO_4$ | 3 A $g^{-1}$ | 249 F $g^{-1}$ | **6** |
| 7 | $[Cu^{I}_4H_2(btx)_5(PMo_{12}O_{40})_2]\cdot 2H_2O$ | 1 M $H_2SO_4$ | 2 A $g^{-1}$ | 237.0 F $g^{-1}$ | **7** |
| 8 | $[Cu^{I}_4H_2(btx)_5(PW_{12}O_{40})_2]\cdot 2H_2O$ | 1 M $H_2SO_4$ | 2 A $g^{-1}$ | 100.0 F $g^{-1}$ | |
| 9 | $RGO/PIL/PMo_{12}O_{40}$ | 0.5 M $H_2SO_4$ | 10 mV $s^{-1}$ | 456 F $g^{-1}$ | **8** |
| 10 | $HT\text{-}RGO\text{-}PMo_{12}O_{40}$ | 1 M $H_2SO_4$ | 10 mV $s^{-1}$ | 276 F $g^{-1}$ | **9** |
| 11 | $[Cu^{II}_2(bipy)(H_2O)_4(C_6H_5PO_3)_2Mo_5O_{15}]$ | 0.5 M $H_2SO_4$ | 2 A $g^{-1}$ | 160.9 F $g^{-1}$ | **10** |
| 12 | $(PMo_{12}/PANI/TiN\ NWA)$ | 1 M $H_2SO_4$ | 1 A $g^{-1}$ | 469 F $g^{-1}$ | **11** |

**Table S8** Specific Capacitance of various components.

| | **Cu+$SiMo_{12}$** | **$SiMo_{12}$+$L_1$** | **$SiMo_{12}$** | **Acetylene** | **4–** | **1–** |
|---|---|---|---|---|---|---|

| | +$L_1$+$L_2$ | +$L_2$ | @TBAB | black | GCE | GCE |
|---|---|---|---|---|---|---|
| 2 A $g^{-1}$ | 249.1 | 172.5 | 146.9 | 1.12 | 1208.7 | 1618.4 |
| 5 A $g^{-1}$ | 204.7 | 152 | 69.3 | 1.07 | 821.7 | 1398 |
| 10 A $g^{-1}$ | 190.7 | 144 | 61.3 | 0.93 | 620 | 1287.3 |
| 15 A $g^{-1}$ | 186 | 141.3 | 50 | 0.9 | 579.3 | 1199.5 |
| 20 A $g^{-1}$ | 181.3 | 140 | 42.7 | 0.89 | 523.3 | 1164.2 |

1. Z. Y. Li, Q. Zhang, H. T. Liu, P. He, X. D. Xu and J. H. Li, Organic–inorganic composites based on room temperature ionic liquid and 12-phosphotungstic acid salt with high assistant catalysis and proton conductivity, *J. Power Sources*, 2006, **158**, 103.
2. R. J. Sengwa, S. Choudhary and S. Sankhla, Low frequency dielectric relaxation processes and ionic conductivity of montmorillonite clay nanoparticles colloidal suspension in poly (vinyl pyrrolidone)-ethylene glycol blends, *Express Polym. Lett.*, 2008, **2**, 800-809.
3. E. Jaimez, G. B. Hix and R. C. T. Slade, The titanium (I) salt of N, N-(diphosphonomethyl) glycine: synthesis, characterisation, porosity and proton conduction, *J. Mater. Chem.*, 1997, **7**, 475-479.
4. X. Xu, Y. P. Zhang, J. Ying, L. Jin, A. X. Tian and X. L. Wang, POM-based compounds modified by mono- and bis-triazole derivatives: photocatalytic, electrochemical, and supercapacitor properties, *CrystEngComm*, 2022, **24**, 1267.
5. S. Roy, V. Vemuri, S. Maiti, K.S. Manoj, U. Subbarao and S. C. Peter, Two Keggin-based isostructural POMOF hybrids: synthesis, crystal structure, and catalytic properties, *Inorg. Chem.*, 2018, **57**, 12078−12092.
6. D. F. Chai, J. J. Xin, B. N. Li, H. J. Pang, H. Y. Ma, K. Q. Li, B. X. Xiao, X. M. Wang and L. C. Tan, Mo-based crystal POMOFs with a high electrochemical capacitor performance, *Dalton Trans.*, 2018, **48**, 13026-13033.
7. D. F. Chai, C. J. Gómez García, B. N. Li, H. J. Pang, H. Y. Ma, X. M. Wang and L. C. Tan, Polyoxometalate-based metal-organic frameworks for boosting electrochemical capacitor performance, *Chem. Eng. J.*, 2019, **373**, 587-597.
8. M. H. Yang, B. G. Choi, S. C. Jung, Y. K. Han, Y. S. Huh and S. B. Lee, Polyoxometalate-coupled graphene via polymeric ionic liquid linker for supercapacitors, *Adv. Funct. Mater.*, 2014, **24**, 7301-7309.
9. J. Suárez-Guevara, V. Ruiza and P. Gómez-Romero, Stable graphene-polyoxometalate nanomaterials for application in hybrid supercapacitors, *Phys. Chem. Chem. Phys.*, 2014, **16**, 20411-20414.
10. B. R. Lu, S. B. Li, J. Pan, L. Zhang, J. J. Xin, Y. Chen and X. G. Tan, pH-

controlled asembly of five new organophosphorus strandberg-type cluster-based coordination polymers for enhanced electrochemical capacitor performance, *Inorg. Chem.*, 2020, **59**, 1702−1714.

11. L. Lu and Y. B. Xie, Fabrication and supercapacitor behavior of phosphomolybdic acid/polyaniline/titanium nitride core–shell nanowire array, *New J. Chem.*, 2017, **41**, 335-346.